MEASUREMENTS OF COLLECTIVE EFFECTS RELATED TO BEAM COUPLING IMPEDANCE AT SIRIUS

F. H. de Sá*, M. B. Alves, L. Liu, Brazilian Synchrotron Light Laboratory, Campinas, Brazil

Abstract

SIRIUS is the new storage-ring-based 4th generation synchrotron light source built and operated by the Brazilian Synchrotron Light Laboratory (LNLS) at the Brazilian Center for Research in Energy and Materials (CNPEM). In ultralow emittance storage rings such as SIRIUS, the small radius of the vacuum chamber gives rise to strong beam coupling impedances which significantly alter the beam dynamics. In this work, we present the single-bunch measurements made so far to characterize such effects and compare the results with those simulated using the impedance budget built during the storage ring design.

INTRODUCTION

SIRIUS is the new Brazilian synchrotron light source based on a 3 GeV electron storage ring, comprising a 20-cell 5BA magnetic lattice with 250 pm rad emittance. It is one of the three 4th generation storage-ring-based light sources in operation worldwide. Information regarding the commissioning results and current operation status can be found in references [1, 2].

The standard storage ring vacuum chamber is cylindrical with 12 mm of inner radius and made of copper. Almost all chambers are coated with non-evaporable getter (NEG) [3, 4] with a thickness of 1.0 μm, including all five 6 mm-gap aluminum chambers for the commissioning undulators [5]. Such small chambers give rise to strong beam coupling impedances not only due to the finite conductivity of the materials, but also because of inner transitions and cross section changes originated by special devices. For this reason, the design of every device of the storage ring was optimized not only based on its vacuum performance but also on the additional impedance it creates [6–11].

Details about the impedance budget can be found in references [12, 13]. The resistive wall and longitudinal coherent synchrotron radiation impedances and wakes were evaluated using semi-analytical approaches [14, 15] and refer to the system response to a point-like charge, which may turn time-domain simulations challenging due to the longitudinal grid discretization. For this reason all these wakes were convoluted with a 40 μm Gaussian distribution to remove high frequency components. On the other hand, the geometric wakes were computed using numerical solvers of Maxwell equations [16–19] and thus refer to the system response to a Gaussian bunch. Since in this work we will deal with single-bunch effects, all simulations were performed with a wake-length of 0.4 m and a source bunch with length of 0.5 mm. They were used as it is in time-domain simulations and their impedances were calculated up to 150 GHz

---
* fernando.sa@lnls.br

for frequency domain simulations. The impedance budget used here reflects the current status of the machine, including models for all in-vacuum components, except one: the temporary Petra 7-Cell cavity that is currently being used. Instead, the broadband contribution of the still not installed superconducting cavities is included.

It is important to note that all comparisons of the results predicted by the impedance budget with measurements presented in this work were performed using the impedances and wakes calculated directly from 2D and 3D models of the vacuum chamber components, without any kind of fitting of effective models such as resonators, resistive and inductive impedances or scaling of the budget to fit the data. The main idea is not only to characterize the storage ring and create a model to describe its dynamics, but also to evaluate the methodology applied along the last few years to compose the impedance budget and to have an indication of how predictive this kind of approach could be for future machines and also for the next components to be installed in the storage ring.

LONGITUDINAL DYNAMICS

We performed bunch length measurements with a recently installed Hamamatsu C5680 dual-axis streak camera in two occasions. The first data set (Data Set 1) was acquired with a single-bunch in the machine using the streak camera in single scan mode in its highest resolution configuration. The bunch charge was varied by inducing partial current losses with our horizontal pinger and the bunch distribution was retrieved as function of the current. The second data set (Data Set 2) was acquired with a different setup: two bunches were injected, one in bucket 1 with high initial charge (2.3 mA) and other in bucket 431 with very low current (20 μA). Since the fast scan frequency of our camera is 1/4 of the RF frequency, it is possible to see every other bucket simultaneously with alternating vertical positions on the camera. With this setup we can not only measure the longitudinal distribution of the high charge bunch, but also its synchronous phase variation with current, since the low charge bunch serves as a time reference. This idea was already discussed in the literature [20] and it is known for compensating jitter between the RF system and the synchroscan unit of the camera, so that the average position of both bunches provide the synchronous phase shift information of the high charge one. The disadvantage of this setup is that the resolution for bunch length is compromised because we need to operate the camera with a different scale to see both bunches.

In both scenarios the measurements were performed with an integration time of 100 ms to improve resolution. Even though this long exposure time does increase the measured
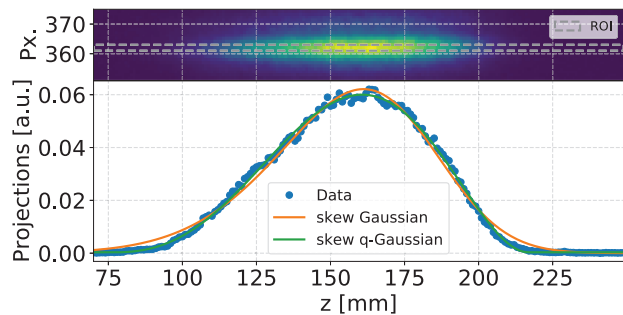
Figure 1: Summary of data analysis setup, showing the small Region Of Interest (ROI) used to project the data and the different performances of the skew Gaussian and skew q-Gaussian p.d.fs on data fitting.

bunch length due to synchrotron oscillations averaging, we expect this effect to be small, considering that previous measurements of longitudinal phase stability indicated it to be better than 10 % of the natural bunch length. The second data set was taken almost one month later than the first one such that the experimental setup underwent improvements in this meantime, mainly with the installation of a 10 nm band-pass filter at 650 nm. This factor may indicate the second data set is more reliable, but other important aspects such as the optical focusing and slit sizes were well tuned in both experiments. The size of the slit was also measured with the camera in focus mode (without synchroscan) so that it could be used to deconvolute the measured bunch sizes.

The analysis of the data was also a point of careful interpretation. In order to make comparisons with the model more reliable, we did not compute the bunch statistics directly from the measured distribution. Computation of higher central moments using data points is very prone to errors originated from fluctuations in the distributions tails, especially for low currents where signal-to-noise ratio is smaller. Besides, instead of projecting the full image of the beam to estimate the distribution, we extract the information only from a very thin central slice, losing data averaging, but not compromising the estimated distribution with noise or imperfections of the slit. Figure 1 shows this analysis setup. The resulting projection was then fitted with known probability density functions (p.d.f) and the first and second moments were calculated numerically from them. Regarding the fitting procedure, there are two key aspects for which we paid extreme attention and tried to capture: the thickness of the distribution tails, which influences the values of the higher order central moments, and the skewness of the distribution, introduced by the resistive part of the impedance as the bunch current increases. To address the first issue we used a generalization of the Gaussian distribution, namely q-Gaussian [21, 22], defined by:

$$p_q\left(\frac{x-\mu}{\sigma}\right) = \frac{1}{Z_q(\sigma)}\left[1 - \frac{1-q}{3-q}\left(\frac{x-\mu}{\sigma}\right)^2\right]_+^{\frac{1}{1-q}} \quad (1)$$

with $q < 3$ and $q \neq 1$, where σ and μ are free parameters, $Z_q(\sigma)$ is a normalization constant and $[\cdot]_+ = \max(\cdot, 0)$.

This function was also used recently to fit bunch profiles at LHC [23]. The parameter q defines whether the distribution will have heavier ($q > 1$) or lighter ($q < 1$) tails than the standard Gaussian ($q \to 1$). In this work we fixed $q = 1/2$ because the measured distribution presented lighter tails, as can be seen in Fig. 1. To address the second issue we used a skew version of the q-Gaussian p.d.f, which can be defined as [22]:

$$p_q\left(\frac{x-\mu}{\sigma};\alpha\right) = 2p_q\left(\frac{x-\mu}{\sigma}\right)P_q\left(\alpha\frac{x-\mu}{\sigma}\right) \quad (2)$$

where P_q is the cumulative distribution function of the q-Gaussian and α is called skew parameter.

On the other hand, the effects predicted by the model were calculated considering intrabeam scattering (IBS) and impedance simultaneously in a very simplified way. The IBS contribution was calculated by evolving the natural equilibrium emittances in time until convergence using the analytic formulas of Bjorken-Mtingwa [24] for the growth rates. The underlying model of the storage ring used in this calculation was one that fits the measured vertical dispersion function ($|\vec{\eta}_y|_{\text{BPMs}} = 5$ mm) and the global betatron coupling strength $|C| = 0.011$. Considering the current working point of the storage ring (49.078, 14.139), this model predicts an emittance ratio at zero current of $\varepsilon_2/\varepsilon_1 = 2.0$ %, where $\varepsilon_{1,2}$ are the two equilibrium emittances of the transverse eigenmodes of the one-turn map. The impedance budget effect was evaluated by solving the Haissinski equation [25] for the longitudinal distribution, $\rho(z)$. In order to account for the mutual influence of both effects (IBS and wakes) we performed the following iterative scheme for each bunch current:

$$(\sigma_\delta, d, \mu_2) \leftarrow (\sigma_{\delta 0}, \sigma_{\delta 0} + 2\epsilon, \text{HAI}(\sigma_{\delta 0}))$$
$$\textbf{while } |d - \sigma_\delta| < \epsilon \textbf{ do}$$
$$\quad (d, \sigma_\delta) \leftarrow (\sigma_\delta, \text{IBS}(\mu_2))$$
$$\quad \mu_2 \leftarrow \text{HAI}(\sigma_\delta)$$
$$\textbf{end while}$$

where d is a dummy variable, $\sigma_{\delta 0}$ is the natural energy spread, ϵ is some convergence tolerance (10^{-7} was used), $\mu_2 = \langle z^2 \rangle - \langle z \rangle^2$ is the second central moment of $\rho(z)$ and the operators IBS($\cdot$) and HAI($\cdot$) represent the IBS and Haissinski solvers. This algorithm takes approximately three iterations to converge and the final σ_δ, $\rho(z)$ as well as the equilibrium emittances are retrieved for each current. It is worth noting that at all iterations the natural equilibrium parameters are used as initial conditions for IBS($\cdot$), not to account for the same effect twice, and that in all steps the growth rates were calculated under the assumption of Gaussian distribution, even though the longitudinal distribution clearly does not satisfy this condition.

Figure 2 shows the measurements and the model results for the longitudinal distribution, bunch length and synchronous phase shift as a function of the current. We notice that the bunch lengthening and distribution profiles predicted by the model are in very good agreement with the measured data from Data Set 1, which was acquired with a higher time resolution scale. However, the difference between the
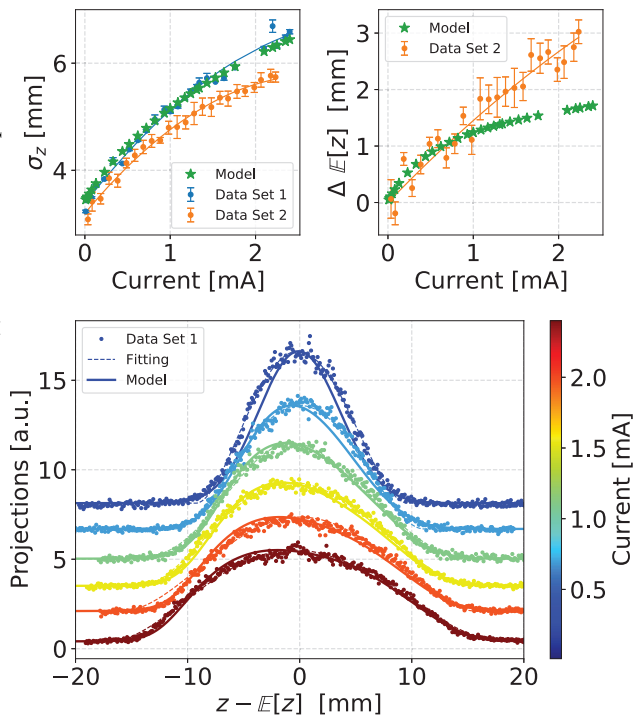
Figure 2: Comparison of distribution profile, bunch length and synchronous phase shift measurements with model predicted values.
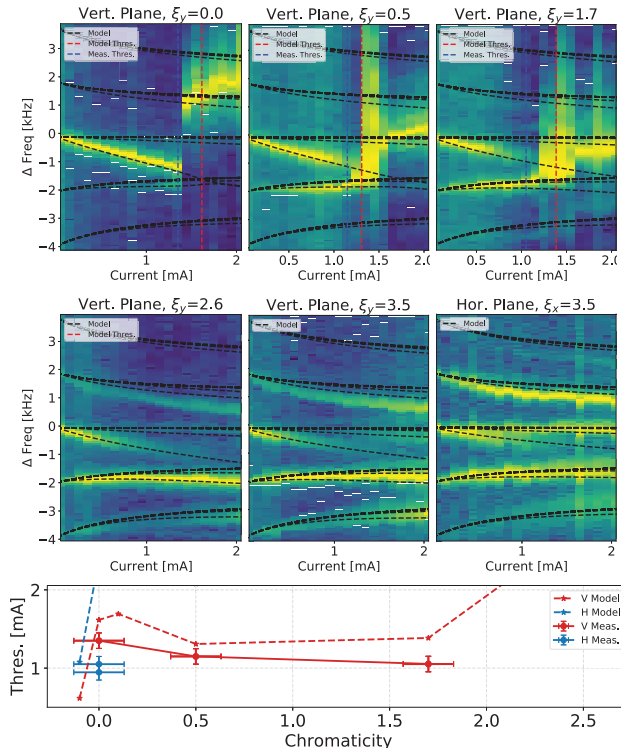

Figure 3: Comparison of measured single-bunch tune-shifts and instability thresholds as function of current and chromaticity with model predicted values.

two measurements needs further investigation in the future. The discrepancy observed in synchronous phase shift is not fully understood yet, but might be related to the absence of the impedance of the Petra 7-Cell cavity in our budget or to imprecision of the measurement. Since this is a very sensitive experiment, we will repeat it in future works and try to compare it with other methods. While the bunch distribution is a key factor to calculate other observables of the machine, such as transverse instabilities and lifetime [26], the synchronous phase shift does not share this far reaching influence.

TRANSVERSE DYNAMICS

We also measured the transverse frequency response of a single-bunch as function of the current for different values of chromaticity to access instability thresholds and tune-shifts. We achieved this by kicking the beam horizontally with our horizontal pinger with an initial amplitude of approximately 25 μrad and acquiring 20 ms of turn-by-turn position data and the spectrum averaged by three consecutive acquisitions with the single-bunch functionality of a iGp12 Dimtel bunch-by-bunch processor [27]. The same setup was repeated for the vertical plane, using the vertical pinger and iGp12 processor. On the other hand, the tune-shifts predicted by the model were calculated using mode-coupling theory [28], considering ±4 azimuthal modes and the first 21 radial modes and using the simulated bunch lengths and distribution-averaged synchrotron frequency as function of current obtained in the previous section. This approach was

crucial to obtain agreement with experimental data. Figure 3 shows that the simulation captures the behavior of the azimuthal modes 0, −1 and −2 with good accuracy for both transverse planes (not all horizontal data are shown since they do not add new information), however the model seems to underestimate the shifts of positive modes. Regarding the instability thresholds, we only detected unstable oscillations at zero chromaticity in the horizontal plane, which is in good agreement with the model considering the uncertainty in the measured chromaticity. For the vertical plane, it seems the model overestimate the threshold by 15 %.

CONCLUSIONS

The impedance budget model proved to be very useful to reproduce the measured bunch lengthening and distribution profiles in the longitudinal plane and the transverse tune-shifts and instability thresholds in the transverse planes. The equilibrium parameters as function of current calculated in this work were also successfully employed to explain Touschek lifetime measurements [26]. The next steps involve characterizing local impedances to access the accuracy of the individual impedance simulations and to perform multi-bunch measurements to map our sources of instability in uniform filling. Currently, we notice a very weak instability in both transverse planes, whose coupled bunch mode decomposition is not fully understood. Another important study is regarding the identification of possible heat sources for future operations with higher currents.

REFERENCES

[1] L. Liu *et al.*, "Status of Sirius Operation", presented at the 13th International Particle Accelerator Conf. (IPAC'22), Bangkok, Thailand, Jun. 2022, paper TUPOMS002, this conference.

[2] X. R. Resende, M. B. Alves, F. H. de Sá, L. Liu, A. C. S. Oliveira, and J. V. Quentino, "Sirius Injection Optimization", presented at the 13th International Particle Accelerator Conf. (IPAC'22), Bangkok, Thailand, Jun. 2022, paper THPOPT038, this conference.

[3] R. M. Seraphim *et al.*, "Vacuum System Design for the Sirius Storage Ring", in *Proc. IPAC'15*, Richmond, VA, USA, May 2015, pp. 2744–2746. doi:10.18429/JACoW-IPAC2015-WEPMA003

[4] R. M. Seraphim *et al.*, "Installation and Commissioning of the Sirius Vacuum System", in *Proc. IPAC'21*, Campinas, Brazil, May 2021, pp. 3455–3458. doi:10.18429/JACoW-IPAC2021-WEPAB333

[5] B. M. Ramos *et al.*, "Aluminum Vacuum Chamber for the Sirius Commissioning Undulators", in *Proc. IPAC'21*, Campinas, Brazil, May 2021, pp. 3467–3470. doi:10.18429/JACoW-IPAC2021-WEPAB336

[6] H. O. C. Duarte, S. R. Marques, and L. Sanfelici, "Design and Impedance Optimization of the SIRIUS BPM Button", in *Proc. IBIC'13*, Oxford, UK, Sep. 2013, paper TUPC07, pp. 365–368.

[7] H. O. C. Duarte and S. R. Marques, "Impedance Optimization of Sirius Stripline Kicker", in *Proc. IBIC'15*, Melbourne, Australia, Sep. 2015, pp. 302–306. doi:10.18429/JACoW-IBIC2015-TUPB006

[8] H. O. C. Duarte, L. Liu, and S. R. Marques, "Evaluation and Attenuation of Sirius Components Impedance", in *Proc. IPAC'17*, Copenhagen, Denmark, May 2017, pp. 3048–3051. doi:10.18429/JACoW-IPAC2017-WEPIK054

[9] H. O. C. Duarte, L. Liu, S. R. Marques, T. M. da Rocha, and F. H. de Sá, "Analysis and Countermeasures of Wakefield Heat Losses for Sirius", in *Proc. IPAC'17*, Copenhagen, Denmark, May 2017, pp. 3052–3055. doi:10.18429/JACoW-IPAC2017-WEPIK055

[10] H. O. C. Duarte and A. Barros, "Longitudinal Kicker Design for Sirius Light Source", in *Proc. IPAC'19*, Melbourne, Australia, May 2019, pp. 57–60. doi:10.18429/JACoW-IPAC2019-MOPGW002

[11] H. O. C. Duarte, P. P. S. Freitas, A. R. D. Rodrigues, R. M. Seraphim, and T. M. da Rocha, "Design Review of Bellows RF-Shielding Types and New Concepts for Sirius", in *Proc. IPAC'19*, Melbourne, Australia, May 2019, pp. 53–56. doi:10.18429/JACoW-IPAC2019-MOPGW001

[12] F. H. de Sá, H. O. C. Duarte, and L. Liu, "Update of the collective effects studies for Sirius", in *Proc. 8th Int. Particle Accelerator Conf. (IPAC'17)*, Copenhagen, Denmark, May 2017, paper THPAB002, pp. 3680–3683, doi:10.18429/JACoW-IPAC2017-THPAB002

[13] F. H. de Sá, "Study of impedances and collective instabilities applied to Sirius", Ph.D. thesis, Instituto de Física Gleb-Wataghin, Universidade Federal de Campinas, Campinas, Brazil, 2018. http://repositorio.unicamp.br/jspui/handle/REPOSIP/331867

[14] N. Mounet, "The LHC Transverse Coupled-Bunch Instability", Ph.D. thesis, École Polytechinique Fédérale de Lausanne, Lausanne, Swiss, 2012.

[15] J. B. Murphy, S. Krinsky, and R. L. Gluckstern, "Longitudinal wakefield for an electron moving on a circular orbit", *Particle Accelerators*, v. 57, n. BNL-63090, p. 9–64, 1997.

[16] I. Zagorodnov and T. Weiland, "TE/TM field solver for particle beam simulations without numerical Cherenkov radiation", *Phys. Rev. ST Accel. Beams*, vol. 8, p. 042001, April 2005. doi:10.1103/PhysRevSTAB.8.042001

[17] I. Zagorodnov, K. L. F. Bane, and G. Stupakov, "Calculation of wakefields in 2D rectangular structures", *Phys. Rev. ST Accel. Beams*, vol. 18, p. 104401, Oct. 2015. doi:10.1103/PhysRevSTAB.18.104401

[18] ECHO web site, https://echo4d.de/.

[19] GdfidL web site, http://www.gdfidl.de/.

[20] P. F. Tavares *et al.*, "Beam Coupling Impedance Measurements at the ANKA Electron Storage Ring", in *Proc. IPAC'10*, Kyoto, Japan, May 2010, paper TUPD027, pp. 1982–1984.

[21] C. Tsallis, "Possible generalization of Boltzmann-Gibbs statistics", *Journal of Statistical Physics*, vol. 12, pp. 479-487, July 1988. doi:10.1007/BF01016429

[22] M. Tasaki, K. Koike, "On skew q-gaussian distribution", *International Journal of Statistics and Systems*, vol. 12, num. 4, pp. 773–789, 2017.

[23] S. Papadopoulou, F. Antoniou, J. E. Muller, Y. Papaphilippou, and G. Trad, "Modelling and Measurements of Bunch Profiles at the LHC Flat Bottom", in *Proc. IPAC'16*, Busan, Korea, May 2016, pp. 1477–1480. doi:10.18429/JACoW-IPAC2016-TUPMW022

[24] K. Kubo, S. K. Mtingwa, A. Wolski, "Intrabeam scattering formulas for high energy beams", *Phys. Rev. ST Accel. Beams*, vol. 8, issue 8, p. 081001, Aug. 2005. doi.org/10.1103/PhysRevSTAB.8.081001

[25] J. Haissinski, "Exact longitudinal equilibrium distribution of stored electrons in the presence of self-fields", *Nuovo Cim. B*, vol. 18, pp. 72–82, 1973. doi.org/10.1007/BF02832640

[26] M. B. Alves, F. H. de Sá, L. Liu, and X. R. Resende, "Beam Lifetime Measurements in Sirius Storage Ring", presented at the 13th International Particle Accelerator Conf. (IPAC'22), Bangkok, Thailand, Jun. 2022, paper WEPOTK055, this conference.

[27] Dimtel iGp12 bunch-by-bunch processor unit, https://www.dimtel.com/products/igp12

[28] T. Suzuki, "Fokker-Plank theory for transverse mode-coupling instability", *Particle Accelerators*, vol. 20, pp. 79-96, 1986.